Ocean Systems Engineering, *Vol. 15, No. 1 (2025) 43-62*
https://doi.org/10.12989/ose.2025.15.1.043

Development of variable-fidelity FOWT digital twins in extreme sea environments: Part II – high-fidelity CFD analysis

Hyunchul Jang*[1], Hakun Jang[1], Moohyun Kim[2] and Bonjun Koo[1]

[1]*TechnipEnergies, 15377 Memorial Dr, Houston, TX 77079, USA*
[2]*Department of Ocean Engineering, Texas A&M University, Haynes Engineering Building, 727 Ross St, College Station, TX 77843, USA*

(Received December 17, 2024, Revised February 15, 2025, Accepted March 2, 2025)

Abstract. In the coming years, more Floating Offshore Wind Turbines (FOWT) are projected to be installed beyond the continental shelf in the USA and worldwide. Accurate and reliable modeling of various environmental loadings and the resulting dynamic responses are crucial for the structural design, operation, and safety of FOWTs. To develop accurate and reliable FOWT design tools, a collaborative effort between academia (TAMU), industry (Technip Energies), and class society (ABS), supported by the Ocean Energy Safety Institute (OESI), has been undertaken. In this project, accurate and reliable digital twin (DT) models were developed based on high-fidelity CFD models and mid-fidelity potential-flow models. These DT models simulate the coupled dynamics of the floater-turbine-control-mooring system and were validated against 5MW OC3 semisubmersible model test results. The present study is presented in two separate papers. This paper, Part II, focuses on the development and validation of CFD-based high-fidelity DT model for a 15MW semi-submersible wind turbine model. In the high-fidelity coupled analysis methodology, aero-servo-elastic behaviors of the wind turbine blade and tower are simulated by OpenFAST, and the hydrodynamic loads on the floating platform and mooring system are simulated by Technip Energies' CFD-based numerical wave basin tool. The high-fidelity DT simulations were performed for various extreme environmental conditions, and the CFD results were used to calibrate the empirical coefficients of mid-fidelity tools. The development and the validation of mid-fidelity DT models are presented separately in another paper, Part I.

Keywords: Computational Fluid Dynamics (CFD); Floating Offshore Wind Turbine (FOWT); global motion analysis; irregular wave; OpenFAST; numerical wave basin

1. Introduction

Floating Offshore Wind Turbines (FOWTs) represent a pivotal advancement in harnessing renewable energy from offshore wind resources considering stronger and steadier wind in deep water. As these structures evolve to meet growing energy demands, the design and maintenance complexities associated with their dynamic environments necessitate advanced analytical and computational methodologies. Traditional frequency domain approaches, commonly employed for global performance and structural analysis of floating offshore platforms, face challenges in

*Corresponding author, Ph.D., E-mail: Hyunchul.jang@ten.com

http://www.techno-press.org/?journal=ose&subpage=7 ISSN: 2093-6702 (Print), 2093-677X (Online)

accurately capturing the intricate non-linear interactions between the blade, nacelle, tower, and moored substructure inherent in FOWTs.

In response to these challenges, this paper presents a cutting-edge approach: response-based nonlinear time domain analysis, which enhances the precision of FOWT's complex coupled dynamics as a high-fidelity simulation tool. Unlike frequency domain methods, time domain analysis offers a more accurate representation of the dynamic behavior of FOWTs, considering the strong non-linear coupling that defines their mechanical responses. To develop accurate and reliable FOWT design tools, a collaborative effort between academia (Texas A & M University), industry (Technip Energies), and class society (American Bureau of Shipping), supported by the Ocean Energy Safety Institute (OESI), has been undertaken.

A digital twin (DT) is a precise virtual representation of a physical object. It leverages real-time analytics to create virtual models that assess the condition of real systems and identify causal relationships. These virtual models can also forecast outcomes by applying various input parameters expected to occur in real systems soon. Recently, digital twins have been explored as a novel method for predicting wind turbine outputs. Studies on digital twin technology for wind turbines have enhanced operational conditions by developing techniques for fault diagnosis, condition monitoring, and residual life prediction for floating wind turbines. Once a physics-based model is established for the digital twin, it becomes straightforward to analyze and validate various input data and compute complex systems like wind turbines in near real-time.

In this project, accurate and reliable digital twin (DT) models were developed based on the high-fidelity CFD models and mid-fidelity potential-flow models. The present study is presented in two separate papers. Another paper, Part I (Kim *et al*. 2025), focuses on the development and validation of two mid-fidelity DT models (OrcaFlex and OpenFAST-MLTSIM) for a 15MW semi-submersible wind turbine model. Mid-fidelity time-domain analysis tools for wind turbines have been applied in real-world settings, with the results from coupled analyses showing reasonably good agreement when compared to physical model test results. (Koo *et al*. 2013, 2014, Kim *et al*. 2016, 2017, Robertson *et al.* 2023).

This paper, Part II, focuses on the development and validation of CFD-based high-fidelity DT model, and the CFD simulation results were used to calibrate the empirical coefficients of the mid-fidelity tools used in Part I paper (Kim *et al*. 2025). The present high-fidelity DT is for the proof calculation of FOWT design and can include viscous effects and highly nonlinear wave-body interactions, such as wave breaking and impact loads, so that it can replace physical wave-tank experiments.

Traditionally, offshore floater design relies on mid-fidelity tools based on potential theory which need calibration through physical model tests or high-fidelity CFD simulations. Technip Energies (T.EN) has been developing a numerical wave basin tool, a fully integrated analysis tool that includes a CFD solver, potential-based wave models, and a line-dynamics model. This numerical wave basin has been validated against physical model test results for various types of floating platforms and has recently been successfully applied to FOWT applications. The first benchmark validation of the high-fidelity CFD-based coupled analysis tool was conducted in the OC6 CFD JIP initiated by the National Renewable Energy Lab (NREL), aiming to validate 3-hour irregular wave tests using the CFD-based numerical wave basin (Wang *et al.* 2022). Further development of FOWT simulation, considering the dynamics of a wind turbine, has been achieved by Jang *et al*. (2023, 2024). The developed high-fidelity DT was named as Wind Turbine Numerical Wave Basin (WTNWB).

In recent years, CFD analysis has been widely conducted for aerodynamic and hydrodynamic

responses of floating offshore wind turbines by various researchers. Generally, two types of CFD analyses are conducted: uncoupled and coupled analyses. Uncoupled analysis is divided into two subcategories: one focuses on the aerodynamic responses of the wind turbine (Churchfield *et al*. 2012, Gharaati *et al*. 2024), while the other examines the hydrodynamic responses of the floating substructure (Wang *et al.* 2021, 2022, Gu and Chen 2024). The advantage of uncoupled analysis lies in its ability to provide more accurate and reliable aerodynamic or hydrodynamic responses, although it does not account for the dynamic interactions between the two. For coupled analysis, two approaches have been developed: full CFD coupling and hybrid-type CFD coupling. In full CFD coupling, both aerodynamic and hydrodynamic responses are predicted within the CFD solver (Liu *et al.* 2017, Tran and Kim 2016). In hybrid-type coupled analysis, either the aerodynamic or hydrodynamic response is directly solved using the CFD solver, while the other is analyzed using a mid-fidelity analysis tool (Jang *et al*. 2023, 2024; Alonso *et al*. 2023). Although full CFD coupling is highly detailed, it is prohibitively expensive and impractical for assessing low-frequency motion responses in ocean wave conditions. The hybrid-type coupled analysis leverages the strengths of both models, offering a more balanced approach.

In our hybrid-type coupled-dynamic CFD tool, WTNWB, the aero-servo-elastic coupled dynamics of the nacelle, blades, and tower are simulated by OpenFAST (2022), while the nonlinear hydrodynamic loads on the platform and mooring system are simulated by the CFD-based numerical wave basin. A significant advantage of this tool is its ability to provide high-fidelity information at all necessary locations and times during the design and operation of FOWTs. Additionally, it can directly model the entire target system as it is compared to several drawbacks of physical model testing, such as mooring system truncation, inaccurate dynamic wind generation, and blade scale effects.

2. High-fidelity digital twin model: WTNWB

Technip Energies (T.EN) has been developing a CFD-based numerical wave basin, called Mooring/riser Numerical Wave Basin (MrNWB), which is a fully coupled hydrodynamic motion analysis tool incorporating a CFD solver, potential-based wave models, and a line-dynamics model for mooring/riser system. The numerical wave basin has been validated against physical model test results for various offshore floating platforms such as semisubmersible, tension-leg platform (TLP), Spar, and ship-type FPSO (Baquet *et al*. 2017 & 2019, Wu *et al*. 2014, 2016). The CFD simulation results have been systematically validated from system identifications to 3-hour irregular wave simulations. It has been shown with response spectra and statistics that the CFD simulations well predict the platform's global performance for all frequency ranges. The CFD-based numerical wave basin can serve as a complementary tool to physical wave basin tests for offshore platform design.

The CFD-based numerical wave basin uses a general-purpose commercial CFD software, Star-CCM+, that addresses nonlinear, viscous fluid dynamics with the Navier-Stokes equations and captures free surface interactions using the Volume-of-Fluid (VOF) method. It includes fluid-structure interaction capability using their motion solver (DFBI) tightly coupled with dynamic mesh techniques. Nonlinear irregular waves are modeled using PNWT, T.EN's in-house potential-based wave model based on a finite-element approach. It generates wave components with random phases, calibrated to match the target wave spectrum. The potential wave model is integrated with the CFD solver through the Euler-Overlay Method (EOM) in Fig. 1, merging wave

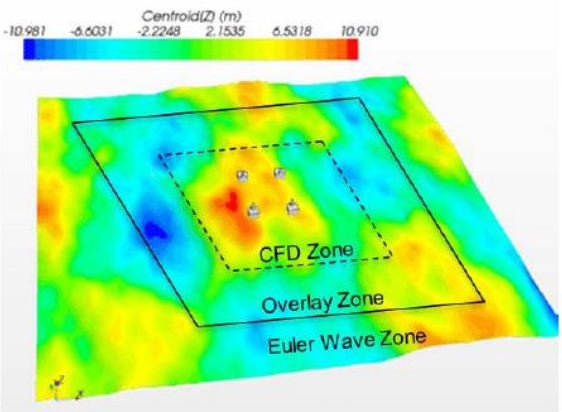

Fig. 1 Schematic of Wave-Coupling Method (Euler-Overlay Method: EOM)

solutions from the outer domain with nonlinear solutions from the CFD solver in the inner domain (Kim *et al.* 2011). Mooring and riser systems are simulated using T.EN's KMOOR software, which is a line dynamics model with springs and lumped masses. The hydrodynamic drag and inertia forces acting on moorings and riser components are determined using the empirical Morison equation. Forces and moments are summed at the hang-off points.

For the coupled analysis of floating offshore wind turbine, the numerical wave basin is tightly coupled with OpenFAST (2022), which is a widely used wind turbine analysis tool developed by National Renewable Energy Laboratory (NREL). The aerodynamic, aeroelastic, and servo-dynamic behaviors of wind turbine are solved by OpenFAST, while the hydrodynamic behavior of the platform subjected to moorings and waves is solved by the numerical wave basin. This novel integrated model is called the Wind Turbine Numerical Wave Basin (WTNWB).

In WTNWB, the CFD solver computes hydrodynamic forces, interacting with wave and mooring models in MrNWB. These loads are transferred to OpenFAST, which resolves platform motions and calculates aerodynamic loads. The platform motion responses are then sent back to the CFD solver to update the mesh. The schematic flowchart illustrating the coupling procedure in the WTNWB is shown in Fig. 2.

3. Validation of high-fidelity DT model

The novel coupled-analysis tool, WTNWB, has been validated using the model test data for the DeepCwind semisubmersible with the NREL 5MW horizontal axis wind turbine (Jang *et al*. 2023, 2024). The model test, conducted at the Maritime Research Institute Netherlands (MARIN), used a 1:50 scale model (Koo *et al*. 2012, Goupee *et al*. 2012, Jonkman *et al*. 2009). A 3-column semisubmersible supported the physical wind turbine]. In the model test, the rotor rpm and blade pitch angle were set according to the tested wind speed. A wind generator with 7 horizontally spaced fans, 5 vertically stacked fans, and a dense honeycomb screen created the required wind field, calibrated using three Acoustic Doppler Velocimeters (ADV) (Ridder *et al*. 2012).

The validation study used a benchmark case based on a 1-year storm condition with an irregular wave following the JONSWAP spectrum (significant wave height of 7.1 m and peak

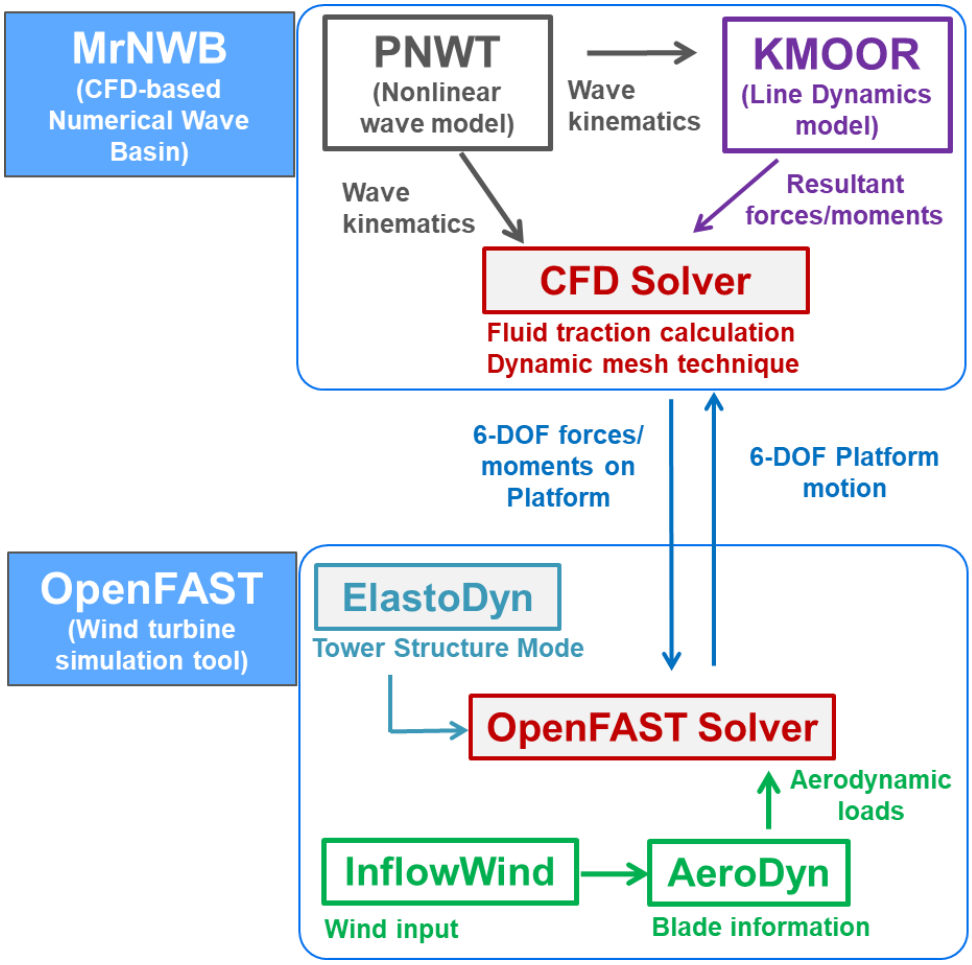

Fig. 2 Schematic Flowchart of Coupling Procedure in Wind Turbine Numerical Wave Basin (WTNWB)

period of 12.1 sec). The study was conducted in colinear wind-wave head seas (180 degrees), with the wind turbine pitch angle and rotor rpm set as in the model test. See the details of the test condition in Table 1. The wind turbine's tower was based on the OC3 Hywind design (Jonkman *et al*. 2010).

The FOWT system properties and setup in WTNWB were verified in a series of system identification tests including static offset tests and free decay tests. A separated wave-only CFD simulation was performed to calibrate the 3-hour non-linear irregular waves, and a separate wind-only OpenFAST simulation was performed to match the wind thrust in the operating condition. The fully-coupled CFD simulation in the 3-hour irregular waves and steady wind accurately predicted platform motion responses. Fig. 3 shows two selected motion responses (surge and pitch) align well with model test data at both motion natural frequency and wave frequency. Fig. 4 illustrates that the spectra for the mooring line tensions simulated by WTNWB are in close agreement with those from the model test. More details of the high-fidelity CFD DT model validation can be found in the references (Jang *et al*. 2023, 2024).

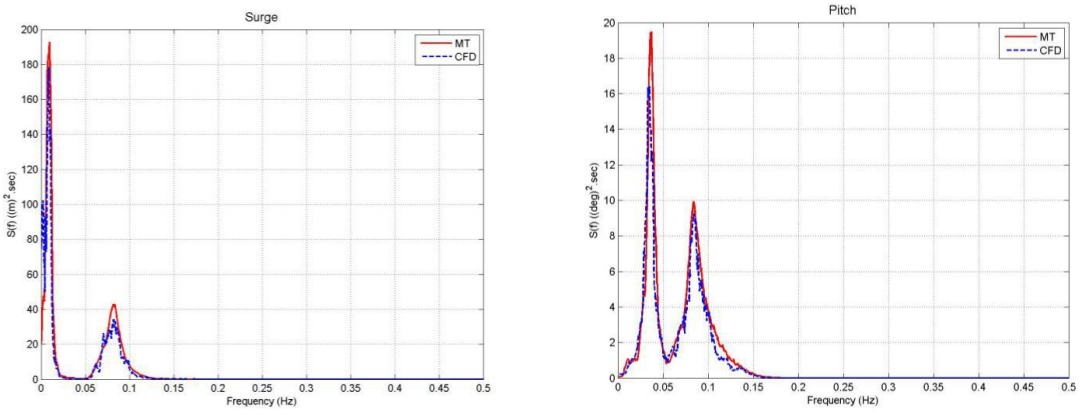

(a) Surge (b) Pitch

Fig. 3 Motion Response in Irregular Wave Test with Steady Wind for DeepCWind Semisubmersible FOWT Validation (MT: Model test, CFD: Numerical Simulation)

Table 1 Benchmark Test Conditions for DeepCWind Semisubmersible FOWT Validation

Item	Unit	Value
Wave Type	**-**	JONSWAP
Significant Wave Height (Hs)	**m**	7.1
Wave Peak Period (Tp)	**m**	12.1
JONSWAP Parameter (g)	**-**	2.2
Wave Heading	**deg**	180
Wind Speed at Hub Height	**m/s**	16.11
Wave Heading	**deg**	180
Rotor Rotational Rate	**rpm**	9.19
Pitch Angle	**deg**	6.4

4. Description of 15 MW FOWT Model

4.1 FOWT model

Fig. 5 shows a schematic of the floating wind turbine platform analyzed in this study with the wind turbine located atop one of the columns. The wind turbine model is based on the IEA 15 MW wind turbine (WT) model. The same Rotor Nacelle Assembly (RNA) is used, but the tower properties are modified to match the modal properties to the T.EN in-house WT model. The WT is supported by T.EN's three-column semi-submersible floating platform design. The WT definitions are summarized in Table 2. For blade pitch, torque, and yaw controls of the wind turbine, the ROSCO controller developed by National Renewable Energy Lab (NREL) is used.

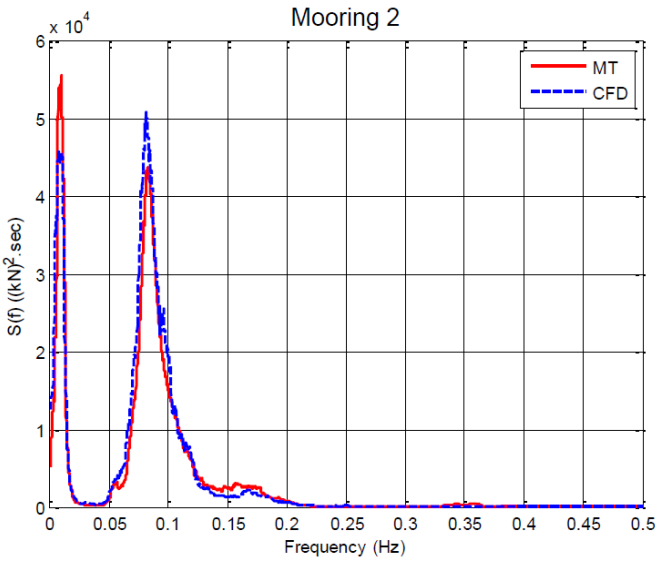

Fig. 4 Mooring (Lee-Side) Tension in Irregular Wave Test with Steady Wind for DeepCWind Semisubmersible FOWT Validation (MT: Model test, CFD: Numerical Simulation)

Fig. 5 Schematic of 15MW FOWT Model

Table 2 15 MW Wind Turbine Specification

Parameter	Unit	Value
Power rating	**MW**	15
Rotor orientation	**-**	Upwind
Number of blades	**-**	3
Control	**-**	Variable speed, collective pitch, yaw
Rated wind speed	**m/s**	10.59
Cut-in wind speed	**m/s**	3.0
Cut-out wind speed	**m/s**	25.0
Rotor diameter	**m**	240
Hub height	**m**	140
Hub diameter	**m**	7.94
Hub overhang	**m**	11.35
Drivetrain	**-**	Low-speed, direct drive
Design tip-speed ratio	**-**	90
Minimum rotor speed	**rpm**	5.0
Maximum rotor speed	**rpm**	7.56
Maximum tip speed	**m/s**	95
Blade mass	**t**	65
RNA mass	**t**	1,017
Tower mass	**t**	860
Tower base diameter	**m**	10

4.2 Mooring system

In the 1000 m water depth case, three taut mooring lines are used. Each mooring leg consists of an upper chain, polyester rope, and bottom chain without any buoyancy module as shown in Fig. 6. The lengths of the upper chain, polyester, and lower chain are 20 m, 1700 m, and 40 m, respectively. The pretensions of mooring lines are 21.5% of MBL. The properties and dimensions of mooring lines are summarized in Table 3.

4.3 Environmental conditions

Table 4 summarizes the selected Design Load Cases (DLCs) based on standard design codes. These load cases are based on met-ocean analysis data for the target site in Northern California, provided by ABS (ABS, 2012). For wind conditions, the analysis uses a 1-hour mean wind speed. The turbulent intensity (TI) for operational conditions and the wind speed for extreme conditions are adjusted according to the 10-minute mean wind speed based on the guidelines from ABS (ABS, 2023).

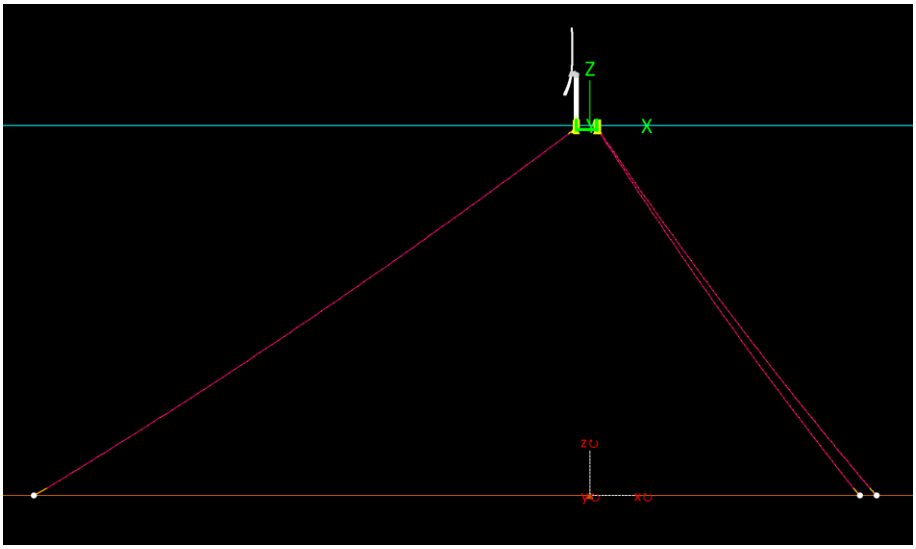

Fig. 6 Mooring Lines Layout

Table 3 Mooring Line Properties and Dimensions

Title		Unit	Value
Water Depth		**m**	1000
Diameter	**Chain**	**mm**	150
	Polyester Rope		259
Length	**Upper Chain**	**m**	20
	Polyester Rope		1700
	Bottom Chain		40
MBL	**Chain**	**kN**	20956
	Polyester Rope		19613
Pretension		**kN**	2000
Horizontal Distance from Fairlead to Anchor		**m**	1462
Mooring Azimuth Angle		**deg**	60/180/300
Departure Angle at fairlead from MWL		**deg**	38.33

5. CFD Setup

The simulations are carried out using commercial CFD software, Star-CCM+ version 17.02, to directly solve the fully nonlinear viscous fluid dynamics governed by Navier-Stokes equations.

Table 4 Environmental conditions for operational and extreme conditions

Title		Unit	Operational	Extreme
Wave	**Hs**	**m**	2.56	12.62
	Tp	**sec**	12	19.96
	gamma	**(-)**	1	1
Current	**Depth - Speed**	**m - m/s**	0 - 0.5 61 - 0.5 91 - 0.1 999 - 0.1	0 - 0.8 90 - 0.8 999 - 0.7
Wind	**Vhub**	**m/s**	10.59	34.58
	TI	**%**	30.73	(-)
	Power Law Coef.	**(-)**	0.14	(-)
	Spectrum		IEC-Kaimal	API-NPD
DLC code			1.3	6.1

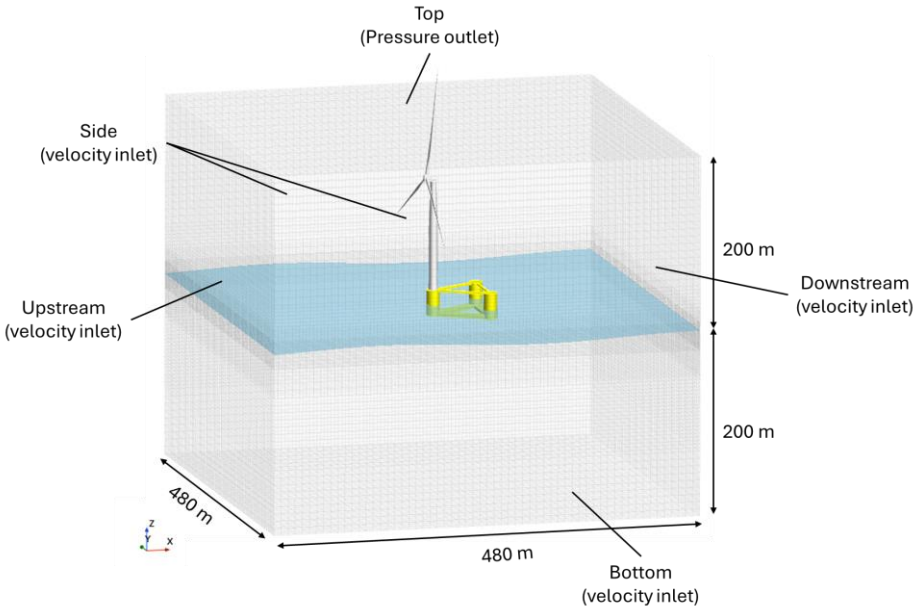

Fig. 7 Computational Domain: Dimensions and Boundary Conditions

The Spalart-Allmaras Detached Eddy Simulation turbulence model is used to resolve unsteady turbulent fluid structures. Three taut mooring lines with the line properties presented in Table 3 are modeled using KMOOR, which has visco-elastic mooring capability.

The CFD computational domain is a cuboid, which is 480 m (L) x 480 m (W) x 360m (D) in size. Note that the tower and wind turbine blades shown in the Fig. 7 are not included in the CFD simulation; they are only depicted to indicate their presence. The velocity inlet boundary condition is prescribed on upstream, downstream, two sides, and bottom boundaries with specified wave

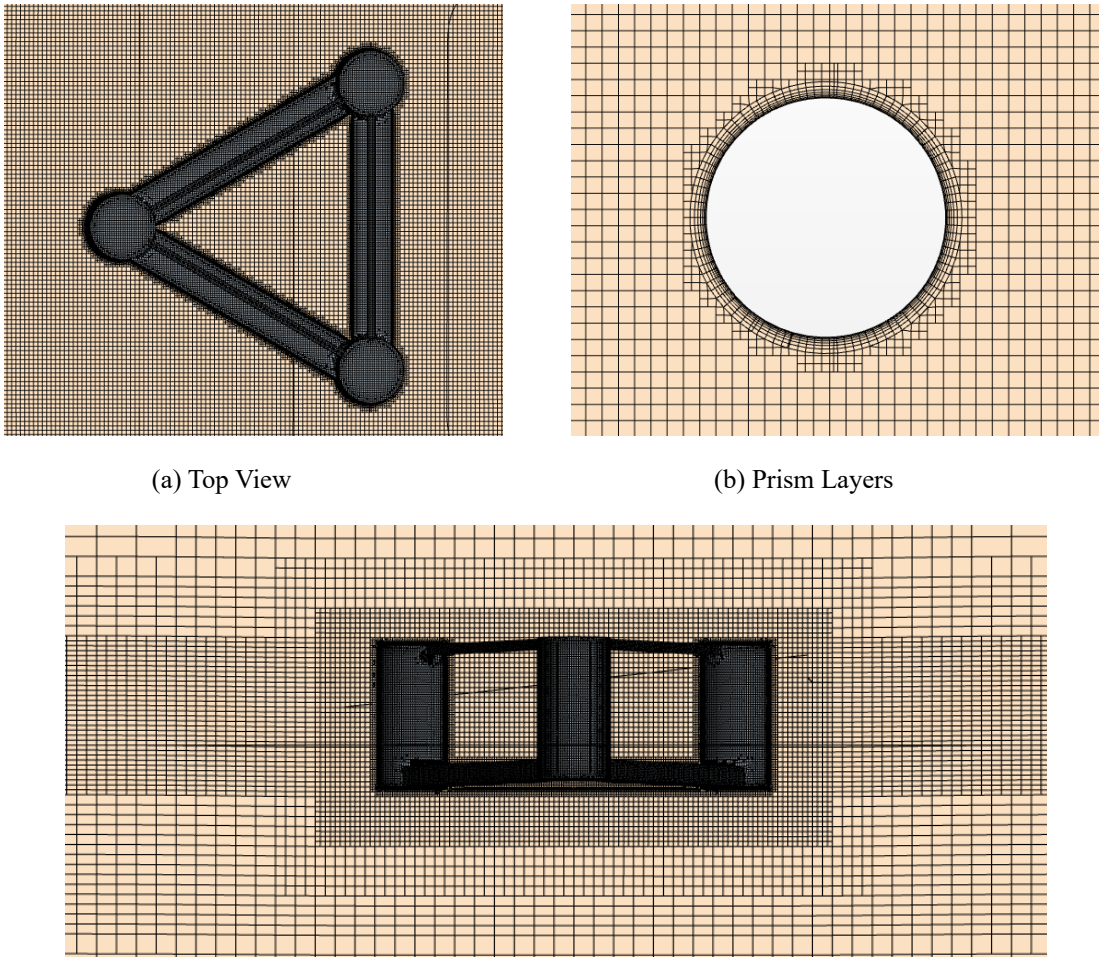

(a) Top View (b) Prism Layers

(c) Side View

Fig. 8 Snapshot of Computational Grid

velocities and volume fractions from the nonlinear wave model. The pressure outlet boundary condition with atmospheric pressure is applied at the top domain boundary, and the no-slip wall boundary condition is used on the semi-submersible body. Near the side boundaries, the overlay zone is located for the EOM approach. The possible mismatch in the wave kinematics between the CFD zone and Euler (Potential) wave zone can be damped out through the overlay zone in the EOM approach.

The grid consists of locally-refined hexahedral cells with refinements near the semi-submersible body and free surface shown in Fig. 8. Prism layer meshes are used adjacent to the body to resolve the boundary layer on the body. The mesh deforms with the 6-DOF platform motion, using algebraic mesh morphing to handle individual mesh movements. The total grid consists of approximately 4 million cells, efficiently handling the dynamic mesh deformation in the irregular wave simulation. The CFD simulation uses an implicit unsteady solver with

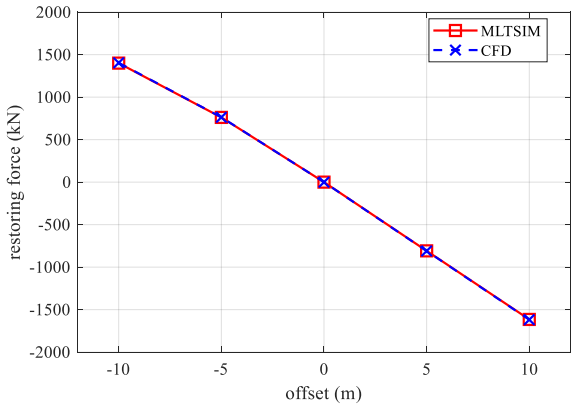

Fig. 9 Static Offset Test Results

second-order time integration, a step size of 0.05 sec, and 8 inner iterations per time step to ensure residual convergence.

The computational mesh deforms according to 6-DOF platform motion, using an algebraic mesh morphing method to handle mesh movements efficiently. The method gradually distorts meshes between near-body and far-body regions while preserving other meshes around the body.

6. System identification tests

The initial system identification tests were conducted to calibrate a mid-fidelity DT model with the high-fidelity CFD-based DT model. As the mid-fidelity DT model, T.EN's proprietary time-domain floater dynamics software, MLTSIM, is used. Mooring stiffness was determined through static offshore testing, while the natural frequency of a FOWT was identified using free-decay tests. In both the mid-fidelity and high-fidelity models, a visco-elastic model is employed to accurately simulate the behavior of the mooring lines. This model accounts for both the elastic and viscous properties of the materials, providing a comprehensive understanding of their dynamic response.

6.1 Static offset test

The mooring lines are composed of a combination of chain, rope, and chain materials, resulting in a system whose stiffness varies based on the extent of stretching. Fig. 9 shows that the restoring force across the range of offsets is in good match in the results.

6.2 Free decay test

In free decay tests, the FOWT in CFD is gradually moved to the imposed initial displacement before being released. In contrast, MLTSIM releases a FOWT from the imposed initial velocity immediately at the start of the simulation.

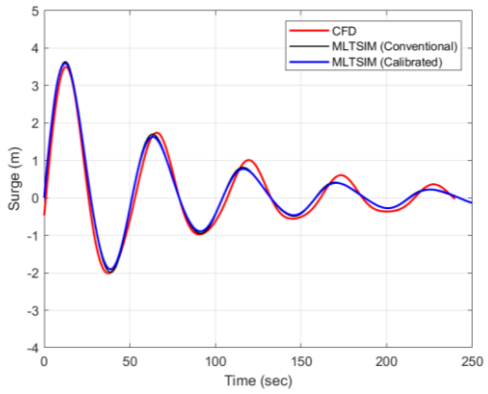

(a) Surge Decay

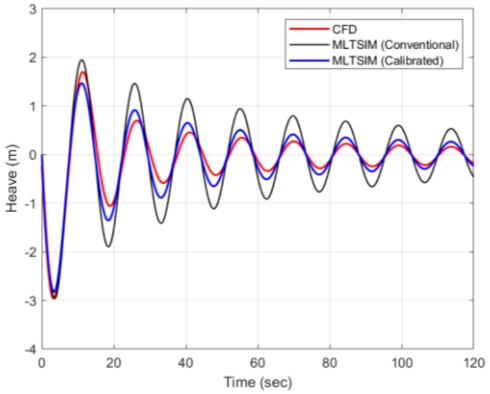

(b) Heave Decay

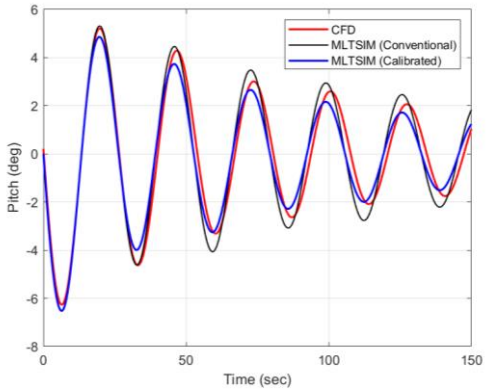

(c) Pitch Decay

Fig. 10 Free Decay Test Results

Table 5 Drag Coefficients for Platform

Title		Cd (Conventional)	Cd (Calibrated)
Column	**Horizontal**	1.0	1.0
	Vertical	1.75	1.1
Pontoon	**Horizontal**	1.0	1.6
	Vertical	1.75	5.0

The drag coefficients were calibrated using the results from CFD simulations, as detailed in Table 5. The details of the methodology to obtain the calibrated drag coefficients are provided in Section 6.3 and 6.4. The motion time series, illustrated in Fig. 10, shows that the two results align well in terms of natural period and damping level after calibrating the drag coefficients. Table 6 summarizes the results of the two simulations. The drag coefficients calibrated in this section are utilized in Part I of this study (Kim *et al*. 2025).

Table 6 Natural Period Comparison in Decay Tests

	Natural Periods (sec)	
	MLTSIM	**CFD**
Surge	54.02	53.65
Heave	14.67	14.66
Pitch	26.53	26.91

Table 7 Vertical Drag Coefficients Calculation

	Unit	**Column**		**Pontoon**	
Amplitude	**[m]**	5	2.5	5	2.5
Period	**[s]**	17	17	17	17
KC	**[-]**	2.13	1.06	3.7	1.85
beta	**[-]**	51852	51852	17220	17220
Re	**[-]**	1.10E+05	5.52E+04	6.36E+04	3.18E+04
Cd	**[-]**	**1.28**	**0.93**	**4.44**	**5.48**

6.3 Vertical drag coefficients

The vertical drag coefficients can be obtained from CFD simulations that incorporate vertically harmonic oscillatory motions. The harmonic oscillation simulations are conducted based on two non-dimensional parameters: Keulegan-Carpenter (KC) number and the frequency coefficient (β). They are defined as follows

$$KC = \frac{U \cdot T_0}{D} = 2\pi \frac{A_0}{D}, \quad \beta = \frac{Re}{KC} = \frac{f_0 \cdot D^2}{\upsilon} \tag{1}$$

where A_0 is the amplitude of oscillation, f_0 is the frequency of oscillation, D is the reference length of the oscillating body, Re is the Reynolds number, and υ is the kinematic viscosity. Two oscillation amplitudes of 2.5 m and 5.0 m are selected, reflecting the heave motion statistics from previous global performance analyses under extreme weather conditions. The oscillation period is chosen to match the heave natural period of 17 seconds. Table 7 presents the oscillation amplitudes, along with their corresponding non-dimensional parameters for both column and pontoon surfaces. Note that the vertical harmonic oscillation simulations should incorporate appropriate free-surface modeling and wave damping techniques at the domain boundaries.

The drag coefficient, C_d, is calculated the following procedure. The hydrodynamic heave force acting on a hull as a result of harmonic oscillation can be described by the following equation

$$-F_z(t) = \delta m \cdot \ddot{z}(t) + \frac{1}{2}\rho A C_d \cdot |\dot{z}(t)|\dot{z}(t) \tag{2}$$

where:

- $F_z(t)$ is the hydrodynamic heave force as a function of time t,
- δm is the added mass coefficient, which accounts for the inertia of the fluid affected by the hull's motion,

- ρ is the fluid density,
- A is the reference area of the hull exposed to the fluid,
- C_d is the drag coefficient, which quantifies the resistance exerted by the fluid,
- $\dot{z}(t)$ is the vertical (heave) velocity,
- $\ddot{z}(t)$ is the vertical (heave) acceleration of the hull.

Eq. (2) is satisfied when the oscillation amplitude is sufficiently large, making the linear damping force negligible compared to the quadratic damping force, which is applicable to our selected test cases. To obtain the drag coefficient C_d, the equation is manipulated by multiplying through by $\dot{z}(t)$ and integrating over an oscillation cycle of the heave motion, from one peak to the next. The resulting integral expression for C_d is

$$C_d = \frac{\int_{t_n}^{t_{n+1}} F_z(t)\cdot\dot{z}(t)dt + 1/2\cdot\delta m\cdot[\dot{z}^2(t_{n+1}) - \dot{z}^2(t_n)]}{-1/2\rho A\int_{t_n}^{t_{n+1}}|\dot{z}(t)|\dot{z}^2(t)dt} \tag{3}$$

where $[t_n, t_{n+1}]$ represents the time interval covering a heave cycle. The numerator of this expression accounts for the work done by the hydrodynamic force during the heave motion and the change in kinetic energy due to the added mass. At the beginning and the end of a heave cycle, the velocity, (ż), is zero, as the cycle is chosen from peak to peak. Consequently, the second term in the numerator becomes zero. This simplifies the equation for C_d to

$$C_d = -\frac{\int_{t_n}^{t_{n+1}} F_z(t)\cdot\dot{z}(t)dt}{1/2\rho A\int_{t_n}^{t_{n+1}}|\dot{z}(t)|\dot{z}^2(t)dt} \tag{4}$$

The drag coefficients are averaged over several oscillation cycles, and the values are presented in Table 7. The drag coefficients in Table 5 were determined between the values obtained from the two harmonic oscillation simulations for the best fit to the CFD simulation results.

6.4 Horizontal drag coefficient

For the horizontal direction, the drag coefficients were determined based on the two reference papers. One is for circular cylinders in oscillatory flow (Sarpkaya 1986), and the other addresses rectangular cylinders (DNV-RP-C205).

For the circular column, two KC numbers were chosen for determining the drag coefficient, as shown in Table 8. According to the physical model test results presented in Fig. 11, the drag coefficient at β = 11,240, which is close to the model scale oscillations for our FOWT model, exhibits KC number dependency. The Cd varies from 0.5 to 1.0 as the KC number ranges from 1 to 2. Since the reference drag coefficient from the physical model test was obtained at the model --scale Reynolds number, the Reynolds number scale effect is also investigated using the surge decay tests. According to the DNV-RP-C205, marine growth for slender structures is between 5 mm to 50 mm. For the full-scale model, a surface roughness of 10 mm is applied to account for the marine growth. With the roughness, the time series in surge decay tests between model-scale and full-scale simulations appear very similar, as shown in Fig. 12(a). For the full-scale simulations, a mesh sensitivity was also performed using a fine mesh with a total of 20 million cells. No mesh

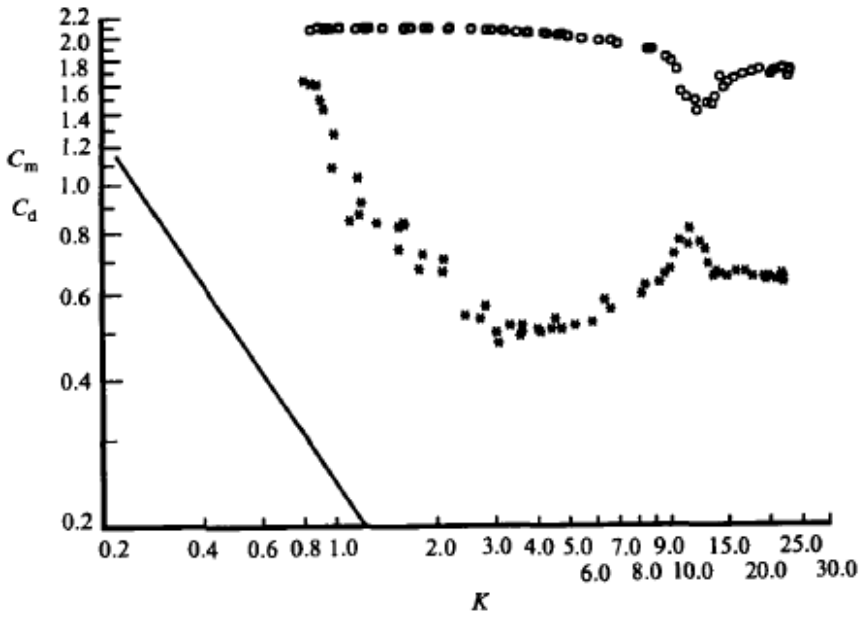

Fig. 11 Drag coefficient for circular cylinder at β=11,240. * symbol represents Cd. (Sarpkaya 1986)

Table 8 Input Parameters for Horizontal Circular Column Drag Coefficients

Amplitude (m)	KC	Beta (Full Scale)	Beta (Model Scale)	Re (Full Scale)	Re (Model Scale)
5	2.13	4.35E+06	1.72E+04	9.27E+06	3.66E+04
2.5	1.06	4.35E+06	1.72E+04	4.63E+06	1.83E+04

sensitivity was observed, as shown in Fig. 12(b). The recommended Cd value is 1.0 at KC = 2 in the model-scale.

For the rectangular pontoon, the drag coefficient was estimated based on "DNV-RP-C205, Appendix E." The recommended Cd value is 1.58 for an aspect ratio L/D = 2.125 for the pontoon.

7. White-noise simulations

White-noise wave test was conducted to identify a FOWT's motion response in irregular waves. In MLTSIM, 200 regular wave components are used to generate the white noise wave. In CFD, the white noise wave is generated using PNWT (Potential-based Numerical Wave Basin), an in-house nonlinear irregular wave tool developed by T.EN. In PNWT, a linear irregular wave input is applied at the inlet of the PNWT, and the waves evolve through the nonlinear potential flow domain. After comparing the wave spectrum at the target location, the energy loss is compensated at the frequency ranges where significant energy loss was observed. The wave elevations and spectra from MLTSIM and CFD inputs look similar but not exactly same, as shown in Fig. 13.

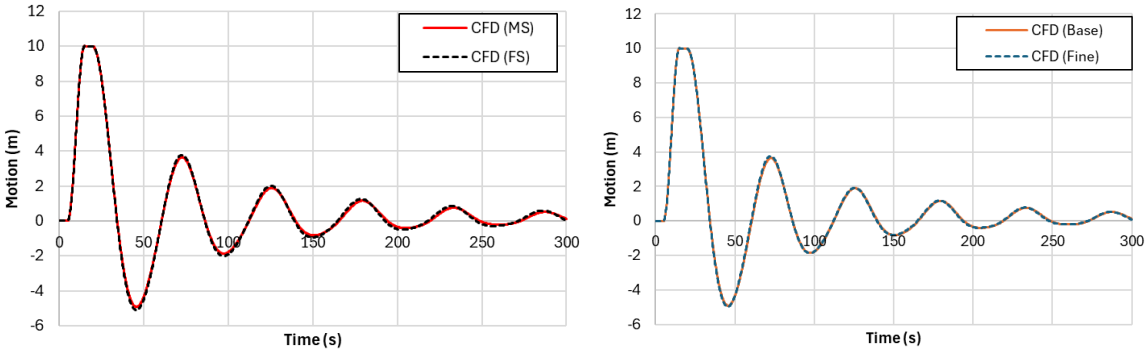

(a) Full-Scale vs Model Scale (b) Mesh Sensitivity test in Full-Scale Simulation

Fig. 12 Scale-Effect in Surge Decay CFD Simulation

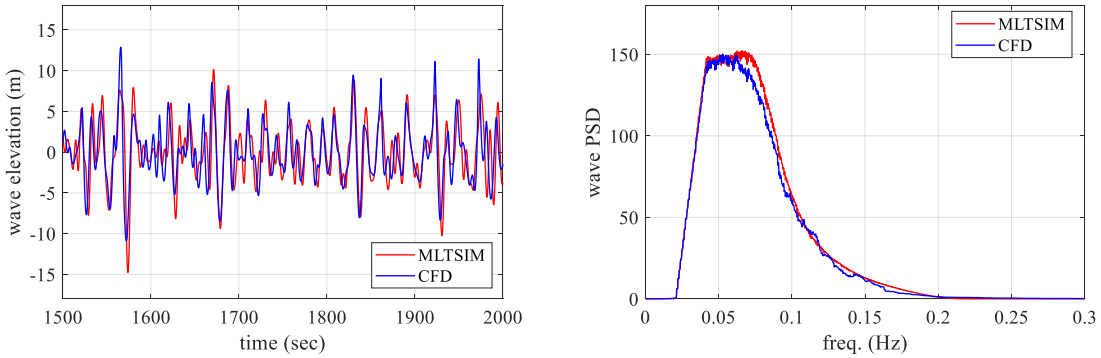

(a) Time Series of White-Noise Wave Elevation (b) Spectrum of White-Noise Wave Elevation

Fig. 13 White-Noise Wave Comparison (Hs=12.62 m)

The white-noise simulations in 1-hour duration were performed at 45-degree wave heading, using both MLTSIM and CFD. The motion spectra and Response Amplitude Operators (RAOs) obtained from this simulation are illustrated in Figs. 14 and 15, respectively. In the surge PSD, low frequencies from 0.01 to 0.03 Hz show a small discrepancy due to nonlinear forces caused by irregular wave forces. In the heave PSD, CFD results indicate higher motion than mid-fidelity results in the frequency range of 0.04 to 0.07 Hz. The pitch PSD matches well in both results. In RAO figures, while the CFD results show marginally higher values for heave at periods exceeding 12 seconds, the overall comparison between MLTSIM and CFD results demonstrates a reasonable agreement, with only minor discrepancies observed. A sensitivity test with vertical drag coefficients in MLTSIM has been performed, but it does not improve the discrepancy in the heave PSD/RAO. The snapshots of White Noise wave test by CFD for 45-deg wave heading are given in Fig. 16.

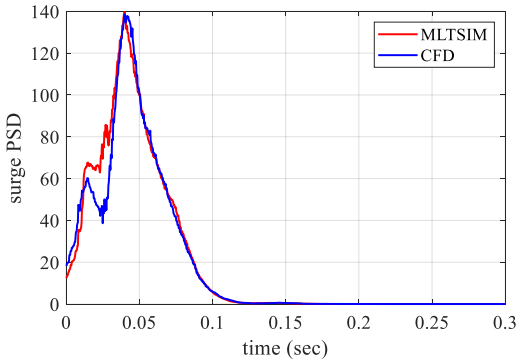

(a) Surge Spectrum

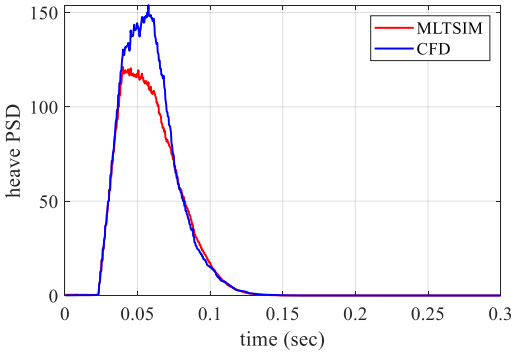

(b) Heave Spectrum

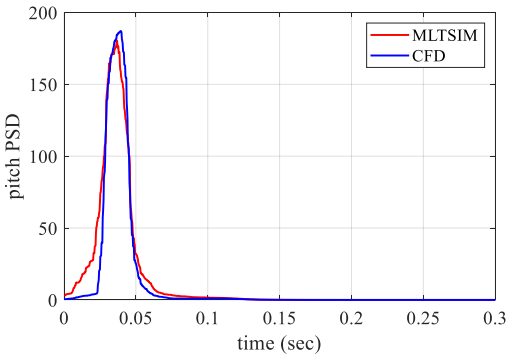

(c) Pitch Spectrum

Fig. 14 Motion PSD in White-Noise Waves (45-deg wave heading)

7. Conclusions

This series of papers introduces a response-based time domain analysis using digital twins to enhance the precision and efficiency of predicting, operating, and analyzing FOWTs. To achieve this, a collaborative effort between academia, industry, and class society has been initiated, supported by the Ocean Energy Safety Institute. The series is divided into two parts: Part I focuses on mid-fidelity models, while Part II delves into high-fidelity CFD-based models.

In this paper Part 2, the high-fidelity DT model, WTNWB, is utilized to investigate a 15MW semi-submersible wind turbine model. This model is capable of providing detailed wind turbine performance metrics, tower structural responses, 6-DOF platform motions, and mooring tensions. System identification tests, including static offset and free decay tests were conducted. After calibrating the mid-fidelity model using results from the high-fidelity model, it was confirmed that both models exhibited similar structural behavior. Additionally, white-noise simulations were conducted to assess the FOWT's response in irregular waves, demonstrating reasonable agreement between MLTSIM and CFD results, with only minor discrepancies observed.

For future work, the study could extend irregular wave tests to include both operational and extreme conditions, capturing a broader range of sea states. This approach would further enhance the understanding and performance of FOWTs.

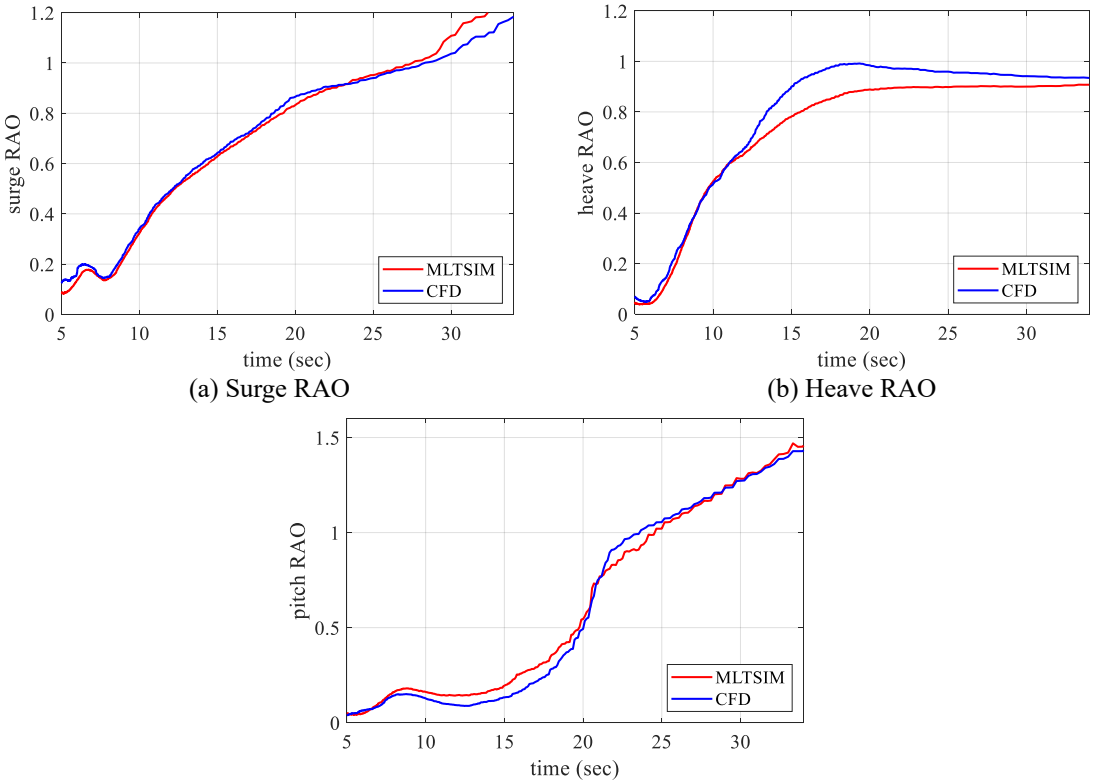

(a) Surge RAO (b) Heave RAO

(c) Pitch RAO

Fig. 15 Motion RAOs in White-Noise Waves (45-deg wave heading)

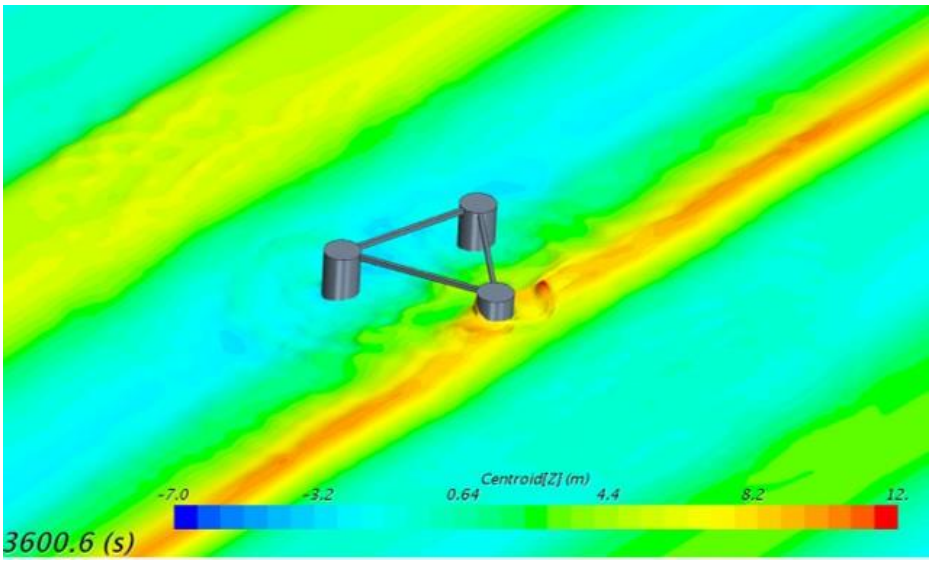

Fig. 16 Snapshots of CFD Simulations in White-Noise Waves

Acknowledgments

The authors would like to thank Ocean Energy Safety Institute (OESI), Texas A&M University (TAMU), Technip Energies (T.EN), and Ekwil for their support and permission to publish this paper. The authors also appreciate Dr. Xiaohong Chen of American Bureau of Shipping (ABS) for her thorough review and recommendation on the present study. Most of CFD simulations presented in this paper have been performed using the Frontera supercomputer at Texas Advanced Computing Center, through the STAR program.

References

Bailey, P.A. (1997), "A unified mathematical model describing the maneuvering of a ship travelling in a seaway", *Trans. RINA*, **140**, 131-149.

Chuang, Z. and Steen, S. (2012), "Speed loss due to seakeeping and maneuvering in zigzag motion", *Ocean Eng*., **48**, 38-46. https://doi.org/10.1016/j.oceaneng.2012.04.009.

Cummins, W.E. (1962), The impulse response function and ship motions (No. DTMB-1661). David Taylor Model Basin Washington DC.

Fang, M.C., Luo, J.H. and Lee, M.L. (2005), "A nonlinear mathematical model for ship turning circle simulation in waves", *J. Ship Res*., **49**(2), 69-79. https://doi.org/10.5957/jsr.2005.49.2.69.

Ferrant, P., Gentaz, L., Monroy, C., Luquet, R., Ducrozet, G., Alessandrini, B. and Drouet, A. (2008), "Recent advances towards the viscous flow simulation of ships manoeuvring in waves", *Proceedings of the 23rd International Workshop on Water Waves and Floating Bodies*, Jeju, Korea.

Fossen, T.I. (2005), "A nonlinear unified state-space model for ship maneuvering and control in a seaway", *Int. J. Bifurcation Chaos*, **15**(9), 2717-2746. https://doi.org/10.1142/S021812740501369.

Hamamoto, M., Matsuda, A. and Ise, Y. (1994), "Ship motion and the dangerous zone of a ship in severe following seas", *J. Soc. Naval Archit. Japan*, (175), 69-78. https://doi.org/10.2534/jjasnaoe1968.1994.69.

Journée, J.M.J. and Adegeest, L.J.M. (2003), Theoretical manual of strip theory program "SEAWAY for Windows". TU Delft Report 1370.

Lee, S.K., Hwang, S.H., Yun, S.W., Rhee, K.P. and Seong, W.J. (2009), "An experimental study of a ship manoeuvrability in regular waves", *Proceedings of the International Conference on Marine Simulation and Ship Maneuverability*, Panama.

Skejic, R. and Faltinsen, O.M. (2008), "A unified seakeeping and maneuvering analysis of ships in regular waves", *J. Mar. Sci. Tech*., **13**(4), 371-394. https://doi.org/10.1007/s00773-008-0025-2.

Son, K.H. and Nomoto, K. (1981), "On the coupled motion of steering and rolling of a high speed container ship", *J. Soc. Naval Archit. Japan*, **150**, 73-83. https://doi.org/10.2534/jjasnaoe1968.1981.150_232.

Stern, F., Agdrup, K., Kim, S.Y., Hochbaum, A.C., Rhee, K.P., Quadvleig, F., Perdon, P., Hino, T., Broglia, R. and Gorski, J. (2011), "Experience from SIMMIAN2008-The first workshop on verification and validation of ship maneuvering simulation methods", *J. Ship Res*., **55**(2), 135-147. https://doi.org/10.5957/jsr.2011.55.2.135.

Xu, Y., Bao, W., Kinoshita, T. and Itakura, H. (2007), "A PMM experimental research on ship maneuverability in waves", *Proceedings of the 26th International Conference on Offshore Mechanics and Arctic Engineering*, American Society of Mechanical Engineers.

Yasukawa, H. (2006), "Simulations of ship maneuvering in waves (1 st report: turning motion)", *J. Japan Soc. Naval Archit Ocean Engineers*, **4**, 127-13.

Zhang, W., Zou, Z.J. and Deng, D.H. (2017), "A study on prediction of ship maneuvering in regular waves", *Ocean Eng*., **137**, 367-381. https://doi.org/10.1016/j.oceaneng.2017.03.046.